



Surface Heat Flux Variations across the Kuroshio Extension as Observed by Surface Flux Buoys

MASANORI KONDA

Department of Geophysics, Graduate School of Science, Kyoto University, Kyoto, and Japan Agency for Marine–Earth Science and Technology, Research Institute for Global Change, Yokosuka, Japan

HIROSHI ICHIKAWA AND HIROYUKI TOMITA

Japan Agency for Marine–Earth Science and Technology, Research Institute for Global Change, Yokosuka, Japan

MEGHAN F. CRONIN

National Oceanic and Atmospheric Administration/Pacific Marine Environmental Laboratory, Seattle, Washington

(Manuscript received 24 August 2009, in final form 18 May 2010)

ABSTRACT

Wintertime sea surface heat flux variability across the Kuroshio Extension (KE) front is analyzed using data from the Kuroshio Extension Observatory (KEO) buoy in the Kuroshio recirculation gyre south of the KE front and from the Japan Agency for Marine–Earth Science and Technology KEO (JKEO) buoy in the north of the front. The coincident data used are from periods during two winters (2007 and 2008), when both buoys had a complete suite of meteorological data. In these two winter periods, the focus of this research is on three types of typical weather patterns referred to here as the northerly wind condition, the monsoon wind condition, and the normal condition. During the northerly wind condition, latent and sensible heat fluxes were large and often varied simultaneously at both sites, whereas during the monsoon wind condition the latent heat flux at the KEO site was significantly larger than that at the JKEO site. The difference between these heat flux patterns is attributed to the different airmass transformations that occur when prevailing winds blow across the KE front versus along the front. Reanalysis products appear to reproduce these heat flux spatial patterns at synoptic scales. It is suggested that the relative frequencies of these different types of weather conditions result in anomalous spatial patterns in the heat fluxes on monthly time scales.

1. Introduction

The Kuroshio and the Kuroshio Extension (KE) contribute to the meridional heat transport system in the Pacific Ocean. Persistent warm surface water in the KE region is considered to be one of the main reasons for the large heat release in fall and winter (e.g., Deser et al. 1999; Qiu et al. 2004). Thus, the strong sea surface temperature (SST) front associated with the KE jet naturally divides the KE region into two subregions. South of the front, a recirculation gyre is found that forms a deep mixed layer during wintertime, where the subtropical mode water (STMW) is ventilated (Masuzawa 1969; Suga

and Hanawa 1990, 1995). In contrast, the region of horizontal mixing between the Oyashio and the KE front is known as the mixed water region (Kawai 1972; Talley 1993; Yasuda 1997; Joyce et al. 2001), where the shallow halocline, due to the excess of precipitation over evaporation, acts as a barrier layer within the isothermal layer (Kara et al. 2000). This north–south contrast of the ocean surface structure can affect the modification of the air mass through changes in the exchange of heat, moisture, and momentum.

The large heat flux in the KE region is correlated with the basin-scale air–sea coupling systems such as the Pacific decadal oscillation (PDO) and other subsequent modes (Mantua et al. 1997; Bond et al. 2003; Kwon and Deser 2007; Di Lorenzo et al. 2008). Previous studies have pointed out that the atmospheric circulation field associated with the sea level pressure (SLP) anomalies in the midlatitudes is correlated with SST anomalies in

Corresponding author address: Dr. Masanori Konda, Dept. of Geophysics, Graduate School of Science, Kyoto University, Kitashirakawa-Oiwake, Sakyo, Kyoto 606-8502, Japan.
E-mail: konda@kugi.kyoto-u.ac.jp

the tropical Pacific on interannual time scales (Tanimoto et al. 1993; Lau and Nath 1994; 1996; Alexander et al. 2002, 2008). Consequently, it is generally accepted that the leading mode of the midlatitude atmospheric variability can be masked by the El Niño–Southern Oscillation (ENSO) signal.

Recent studies, however, have shed light on the role of the extremely large winter evaporative heat release in the KE region on the midlatitude climate (Liu and Wu 2004; Frankignoul and Sennéchaël 2007). Local air–sea interaction analyses have generally focused on either the phase relationship between the sensible (SHF) and the latent heat flux (LHF) and the SST on monthly time scales (Liu and Gautier 1990; Konda et al. 1996; Murakami and Kawamura 2001; Bond and Cronin 2008), or the effects of the SST on the stability of the atmospheric boundary layer (ABL) (Nonaka and Xie 2003; Tokinaga et al. 2006; Tanimoto et al. 2009).

Recently, Nakamura et al. (2008) and Nonaka et al. (2009) suggested from atmospheric general circulation model experiments that the strong restoration of the near-surface air temperature to the SST front affected the activity of the midlatitude storm tracks through the adjustment of the turbulent surface heat flux. Although many surface heat flux datasets show that the area of the large LHF expands to both sides of the KE in cooling seasons (Kubota et al. 2003; Qiu et al. 2004), the boundary layer processes and the oceanic and meteorological parameters are likely to be quite different on either side of the KE. Such a discrepancy suggests a spatial difference in the ocean–atmosphere feedback system in the KE region.

Ninomiya and Mizuno (1985) discussed the spatial pattern of the large LHF in the northwest Pacific associated with northwesterly wind events during wintertime. In particular, lateral advection associated with strong synoptic disturbances in the northwest Pacific can affect the ABL parameters and the underlying SST through air–sea heat exchanges (Lenschow and Agee 1976). Since this landmark study, there has not been a concerted observational study of the influences and structures of these synoptic patterns. However, since June 2004, a surface mooring deployed in the Kuroshio recirculation gyre, referred to as the Kuroshio Extension Observatory (KEO), has been monitoring the air–sea heat, moisture, and momentum fluxes and upper-ocean variations (Cronin et al. 2008). Using the National Centers for Environmental Prediction–National Center for Atmospheric Research (NCEP–NCAR) reanalysis product (Kalnay et al. 1996) and the net air–sea heat flux at KEO as an index, Bond and Cronin (2008) extracted a composite SLP pattern associated with large heat flux at KEO that corresponded to a typical wintertime SLP weather pattern.

In February 2007, the Japan Agency for Marine–Earth Science and Technology (JAMSTEC) deployed a surface flux buoy, the JAMSTEC KEO (JKEO) buoy, on the north side of the KE front. Although there were two gaps due to sensor malfunctions, the JKEO system succeeded in measuring the surface meteorology at 10-min intervals for almost a year. Thus, coincident measurements at KEO and JKEO during the winters of 2007 and 2008 are used in this study to analyze the variations in the ABL parameters and heat fluxes to the north and south of the KE front. In particular, we focus on the variations associated with three different typical wintertime weather conditions and discuss the implications for interannual climate variations.

2. Data and method

The National Oceanic and Atmospheric Administration/Pacific Marine Environment Laboratory (NOAA/PMEL) operates the KEO buoy at 32.4°N, 144.6°E, to the south of the KE front, while JAMSTEC operates the JKEO buoy at 38.0°N, 146.5°E, to the north of the front (Fig. 1). The KEO buoy was first deployed on 16 June 2004, while the JKEO buoy was first deployed on 18 February 2007. For this study, we use data only from the first JKEO deployment period, which ended on 24 March 2008. The study period in which both KEO and JKEO had complete measurements thus spans portions of the winters of both in 2007 and 2008. These winter portions (period I, 18 February–12 March 2007; period II, 1–25 January 2008) will be considered separately.

The KEO and JKEO buoys move within 6 km from the anchor position because of a slack mooring. These buoys were modified based on the Atlas buoy (McPhaden 1995). The meteorological measurement system of the first version (JKEO1) was identical to the KEO system. The variables measured and the available periods of individual data are shown in Fig. 2. They were recorded every 10 min or hourly. Both buoys also measured upper-ocean temperatures as well as salinity (Fig. 2). The current speed was also measured at a depth of 11 m at the JKEO, and the uppermost current meter was mounted at 5 m at the KEO. The latest information of these sites is released on the mooring Web sites (KEO, <http://www.pmel.noaa.gov/keo/>; JKEO, <http://www.jamstec.go.jp/iorgc/ocorp/ktsfg/data/jkeo/>).

SHF and LHF are computed from the high-resolution data using the version 3.0 Coupled Ocean–Atmosphere Response Experiment (COARE) bulk algorithm (Fairall et al. 2003). As the depth of the current meter at JKEO was rather deep to obtain accurate surface currents and the current record at KEO was lost before the end of September (Fig. 2), we could not consider the ocean surface current when computing the wind speed relative to the sea surface. Instead, the average differences in the

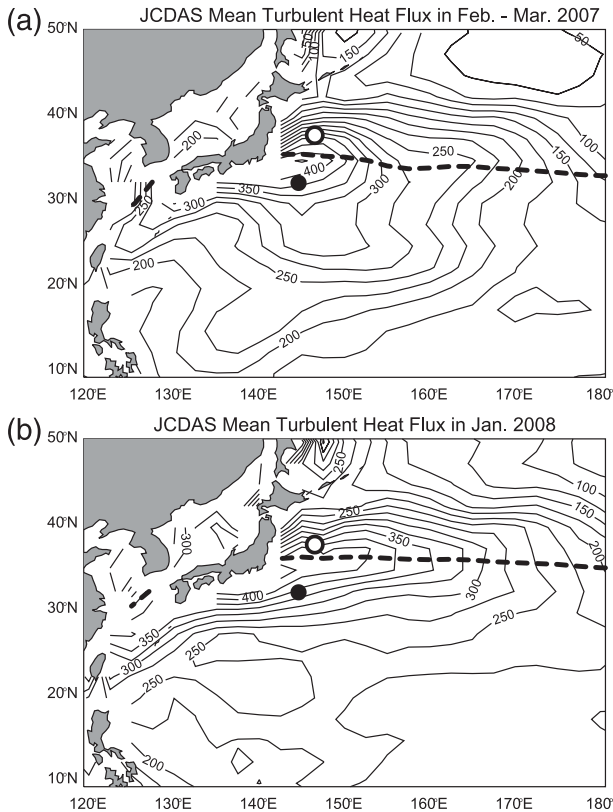


FIG. 1. Mean turbulent heat flux in the northwest Pacific sector during period (a) I and (b) II. Unit is W m^{-2} . The mean value is computed from the equal-weighted accumulation of JCDAS products given every 6 h. Positions of KEO (filled black circle: 32.4°N , 144.6°E) and JKEO (open black circle: 38.0°N , 146.5°E) are overlaid. The 16°C isotherm of the SST is also shown by the thick broken line as a proxy for the SST front associated with the KE jet.

turbulent heat flux with and without the surface current speed were estimated (Table 1) from the COARE 3.0 model and the available current meter record by assuming an eddy viscosity of $1.0 \times 10^{-2} \text{ m}^2 \text{ s}^{-1}$. The uncertainty of the turbulent heat flux caused by the lack of current speed is estimated to be at most 20 W m^{-2} , on average.

As our objective in this paper is to analyze the factors that produce a turbulent heat flux difference between JKEO and KEO, we will decompose the bulk heat transfer equation into terms representing spatial

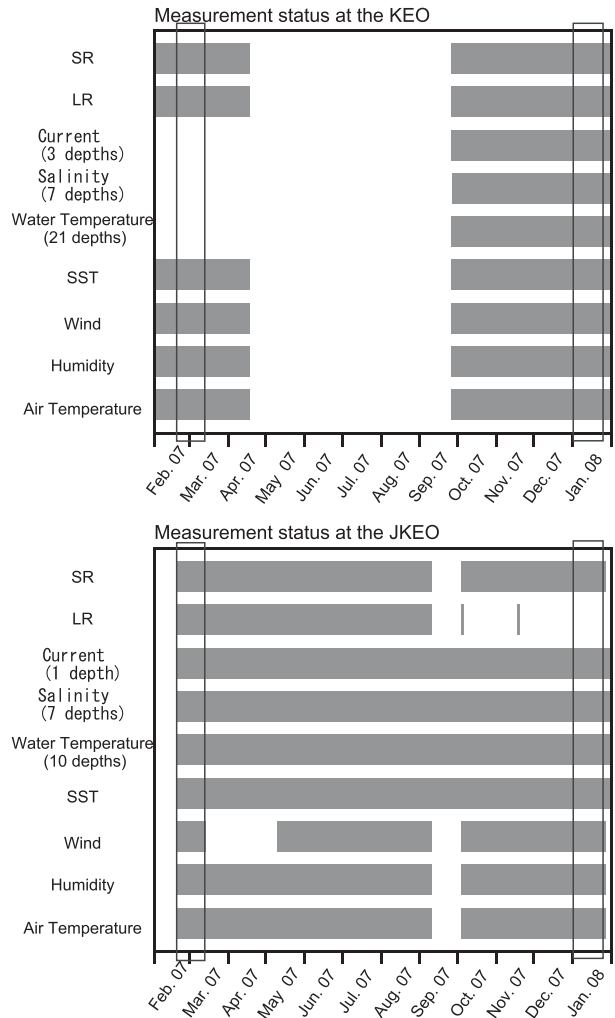


FIG. 2. Periods of data availability for measurements by (top) KEO and (low) JKEO. The shortwave radiation (SR), longwave radiation (LR), ocean current, underwater salinity and temperature profile (water temperature), SST, wind vector (wind), relative humidity (humidity), and air temperature are plotted and shown by gray bars. Thin black squares indicate the ranges of periods I and II.

anomalies of individual ABL parameters. The spatial anomaly of the turbulent heat fluxes is defined in this study as the difference between JKEO and KEO as follows:

$$H' = H^{\text{JKEO}} - H^{\text{KEO}} = \rho C_p C_h^{\text{JKEO}} (T_s^{\text{JKEO}} - T_a^{\text{JKEO}}) U_a^{\text{JKEO}} - \rho C_p C_h^{\text{KEO}} (T_s^{\text{KEO}} - T_a^{\text{KEO}}) U_a^{\text{KEO}} \quad (\text{i})$$

$$= \rho C_p C_h^{\text{KEO}} \left[(T_s' - T_a') U_a^{\text{JKEO}} + (T_s^{\text{KEO}} - T_a^{\text{KEO}}) U_a' \right] \quad (\text{ii})$$

$$+ \rho C_p C_h' (T_s^{\text{KEO}} - T_a^{\text{KEO}}) U_a^{\text{JKEO}} \quad (\text{iii})$$

$$+ R_H \quad (\text{iv})$$

(1)

TABLE 1. Mean and the standard deviation of the differences between the JCDAS heat fluxes and the buoy fluxes at KEO and JKEO. The comparison was made for the daily means of the LHF and SHF individually during periods I and II.

	Period I		Period II	
	KEO	JKEO	KEO	JKEO
Latent heat flux (W m^{-2})	-5.9 ± 41.5	-22.7 ± 40.9	-31.6 ± 50.4	-18.9 ± 5.7
Sensible heat flux (W m^{-2})	-2.0 ± 19.2	5.9 ± 26.8	-4.7 ± 22.5	1.4 ± 16.9

and

$$\begin{aligned}
 Q' &= Q^{\text{JKEO}} - Q^{\text{KEO}} \\
 &= \ell \rho C_e^{\text{JKEO}} (q_s^{\text{JKEO}} - q_a^{\text{JKEO}}) U_a^{\text{JKEO}} - \ell \rho C_e^{\text{KEO}} (q_s^{\text{KEO}} - q_a^{\text{KEO}}) U_a^{\text{KEO}} \quad (\text{i}) \\
 &= \ell \rho C_e^{\text{KEO}} \left[\begin{aligned} &(q'_s - q'_a) U_a^{\text{JKEO}} \quad (\text{ii}) \\ &+ (q_s^{\text{KEO}} - q_a^{\text{KEO}}) U'_a \quad (\text{iii}) \end{aligned} \right] \\
 &\quad + \ell \rho C'_e (q_s^{\text{KEO}} - q_a^{\text{KEO}}) U_a^{\text{JKEO}} \quad (\text{iv}) \\
 &\quad + R_Q, \quad (2)
 \end{aligned}$$

where H and Q , respectively, indicate the SHF and the LHF, and T , q , and U , respectively, denote the temperature, specific humidity and wind speed, with subscripts indicating values at the sea surface (s) and at the height of the meteorological sensors on the buoy hull (a). Superscripts indicate whether the value is at JKEO or KEO and primes indicate the difference between them. Likewise, ρ denotes the density of the atmosphere, C_p the specific heat at constant pressure, and ℓ the latent heat of evaporation. The bulk transfer coefficients of heat and moisture are C_h and C_e , respectively, calculated from the COARE 3.0 model.

Term (i) is the heat flux difference between JKEO and KEO, and terms (ii) and (iii), respectively, show the contributions due to the spatial variations in the air–sea gradients of temperature ($\Delta T'$) and humidity ($\Delta q'$) (where Δ represents the sea – air difference), and due to the spatial variation in wind speed (U'_a). Term (iv) represents the component caused by the spatial variation of the bulk transfer coefficients C'_h and C'_e . The terms of the higher degrees of the spatial anomalies are indicated by R_H and R_Q , respectively.

After analyzing the spatial differences between KEO and JKEO, the regional patterns in the turbulent heat fluxes will be considered using the flux product of the Japan Meteorological Agency Climate Data Assimilation

System (JCDAS), taken from the Japanese 25-Year Reanalysis Project (JRA25; Onogi et al. 2007). The turbulent heat fluxes averaged during the two cold periods in the KE region are shown in Fig. 1. The filled and unfilled black circles show the positions of the KEO and the JKEO buoys, and the thick broken line shows the position of the 16°C SST isotherm as a proxy for the KE front (see Fig. 3d in Chen 2008). Temporal variations of the JCDAS are in good agreement with the buoy measurements (Fig. 2). Summary statistics for periods I and II are listed in Table 2. The standard deviation of the difference amounts to about $40\text{--}50 \text{ W m}^{-2}$, which might be too large to evaluate the difference between the heat fluxes at JKEO and KEO. As the resolution of the product is 2.5° in latitude and longitude, the spatial structure of turbulent heat flux associated with the KE jet or the SST front might be obscured. Therefore, the JCDAS product is used in this study for relating the turbulent heat flux observed at the moored buoys to the spatial patterns on synoptic scales in section 3c.

3. Results

a. Turbulent heat flux variation

The temporal variabilities of the SHF and the LHF during periods I and II measured at JKEO and KEO

TABLE 2. Mean and the standard deviation of the differences between the JCDAS heat fluxes and the buoy fluxes at KEO and JKEO. The comparison was made for the daily means of the LHF and SHF individually during periods I and II.

	Period I		Period II	
	KEO	JKEO	KEO	JKEO
Latent heat flux (W m^{-2})	-5.9 ± 41.5	-22.7 ± 40.9	-31.6 ± 50.4	-18.9 ± 35.7
Sensible heat flux (W m^{-2})	-2.0 ± 19.2	5.9 ± 26.8	-4.7 ± 22.5	1.4 ± 16.9

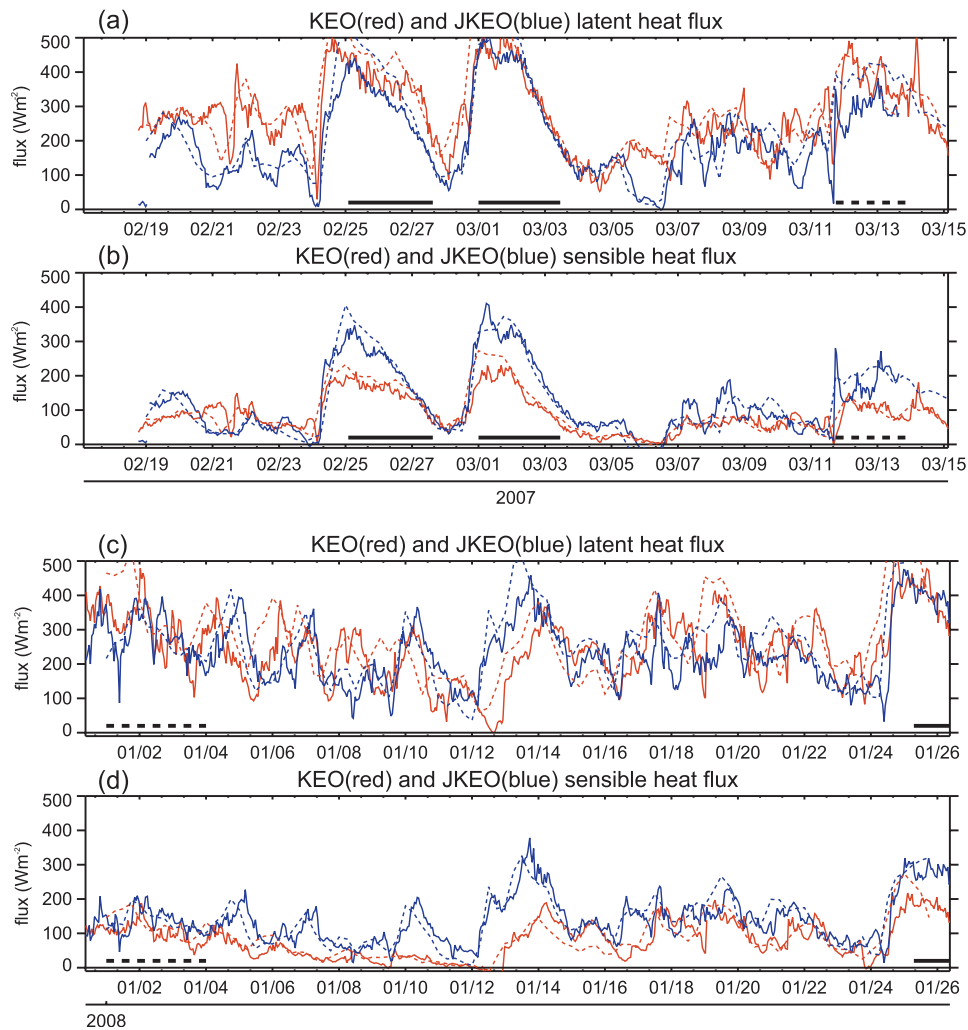


FIG. 3. Time series of the latent and the sensible heat fluxes observed at KEO (red) and JKEO (blue): (a),(b) 19 Feb to 15 Mar and (c),(d) 2 to 26 Jan. Time series of hourly averaged (a),(c) LHF and (b),(d) SHF obtained from the record every 10 min during periods I and II. The values of the JCDAS product on the collocated grid are superimposed by broken lines. Thick black and broken lines indicate the periods of the northerly wind condition and the monsoon wind condition, defined in section 3b, respectively.

(Fig. 3) are generally large on daily to synoptic time scales. During period I, the LHF can be as large as 500 W m^{-2} at the end of February and the beginning of March, both at JKEO and at KEO (Fig. 3a). The LHF shows notably rapid increases in these events. For the rest of period I (the period without the thick lines in Figs. 3a and 3b) the average LHF at JKEO was 155.1 W m^{-2} and that at KEO was 240.8 W m^{-2} , with fluctuations at shorter time scales at the two sites that do not appear to be correlated with each other. The SHF sequence had a larger amplitude at JKEO (Fig. 3b). There are also notable increases in SHF to values of more than 300 W m^{-2} , which were coincident with the increases in LHF. The correlation coefficients between LHF and SHF were 0.91 (KEO) and

0.98 (JKEO). For the rest of the period, the average SHFs at JKEO and KEO were 81.0 and 68.4 W m^{-2} , respectively.

During period II, the LHF occasionally exceeds 400 W m^{-2} , and the LHF and SHF at each buoy also seem to be closely correlated with each other (Figs. 3c and 3d). The correlation coefficients were 0.88 (KEO) and 0.92 (JKEO), respectively. The SHF at the northern buoy (JKEO) was usually larger than that at the southern buoy (KEO). On the contrary, the difference between the LHF at KEO and JKEO fluctuated between positive and negative values during this period. The spatial difference of more than 100 W m^{-2} was observed several times and was associated with the maximum peak of the

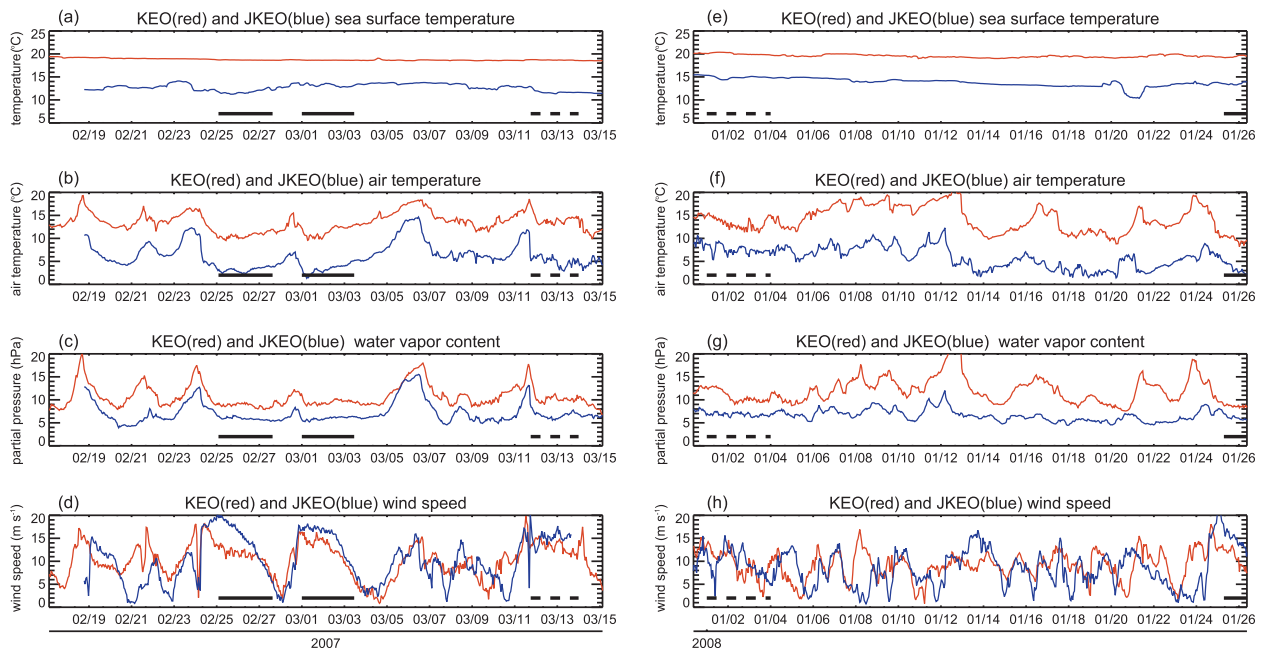


FIG. 4. Time series of the boundary layer parameters observed at KEO (red) and JKEO (blue): (a),(b) 19 Feb to 15 Mar and (c),(d) 2 to 26 Jan. (a) Sea surface temperature, (b) air temperature, (c) water vapor pressure, and (d) wind speed during period I. (e),(h) As in (a),(d), but for period II. Thick solid and broken lines indicate the period for the northerly wind condition and the monsoon condition.

SHF and the LHF. There was stronger high-frequency variability that was less coherent between the sites during period II.

The difference in the climatic conditions between KEO and JKEO are appreciable in the SST, the air temperature, the water vapor content, and the wind speed (Fig. 4). The air temperature and the water vapor content have variabilities at time scales of several days (Figs. 4b,c and 4f,g). Each peak in these parameters of KEO was in good correspondence with that of JKEO during period I, but was less correlated in the last part during period II. These properties are likely to go down to the low values when the turbulent heat flux is extraordinarily high, as shown in Fig. 3. Throughout these periods, the southern buoy (KEO) is generally in a warmer and moister condition than the northern buoy (JKEO).

On the other hand, the wind speed in period II has a notable variability on a short time scale (Figs. 4d and 4h), which seems to affect the variation of the turbulent heat flux (Fig. 3). Throughout periods I and II, we can hardly see any systematic relationship in wind speed between these buoys. Instead, there are some notable events, in which the wind speed at the southern buoy (KEO) eventually becomes much larger than that of the northern buoy (JKEO) by more than 10 m s^{-1} . The spatial difference in the wind speed strongly influences that in the turbulent heat flux. For example, the difference in the turbulent heat flux amounts to 200 W m^{-2}

on 21 February during period I and 8 January during period II (Fig. 3).

Bond and Cronin (2008) showed that the very large LHF and SHF events were associated with an SLP pattern in which the winds at KEO were anomalously northerly. In Fig. 5, we show the time sequence of the wind vector measured at KEO and JKEO during periods I and II. It is obvious in Fig. 5a that both SHF and LHF were maximized almost simultaneously during the strong northerlies beginning on 24 and 28 February, respectively. From 11 March, the wind was almost westerly, possibly associated with the Siberian outbreak that is typical of the winter monsoon. During period II, a simultaneous change between the KEO and JKEO turbulent heat fluxes was observed only at the end of the period from 24 January 2008. For other times, the wintertime heat fluxes at KEO and JKEO seemed to change independently, possibly due to short-term variations of the wind speed.

b. Turbulent heat flux under typical winter weather conditions

When winds are northerly, KEO is located downwind of JKEO. It is well known that winter storms in the KE region are characterized by strong northerly winds (e.g., Ninomiya and Mizuno 1985). During these events, the turbulent heat fluxes at the northern (JKEO) and the southern (KEO) buoys increase almost simultaneously

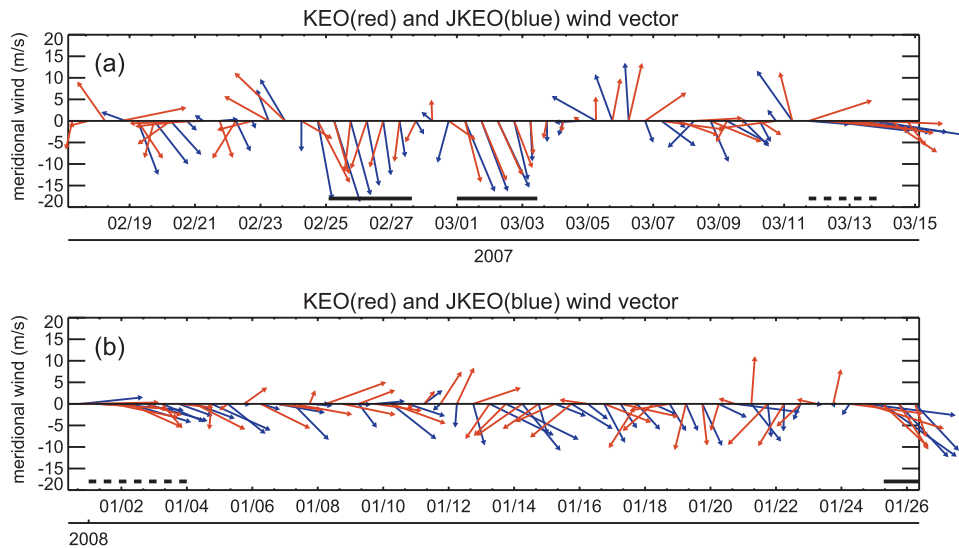


FIG. 5. The vector wind diagram measured at KEO (red arrows) and JKEO (blue arrows) plotted during periods (a) I and (b) II. Each wind vector is the average for 12 h made from the raw record. The vertical axis indicates the meridional component of the wind vector, while the zonal component of the vector follows the vertical scale. Thick black line indicates the period of the northerly wind condition. Thick broken line shows the period of the monsoon wind condition.

(as shown in Figs. 3 and 5), although they are on opposite sides of the SST front. During other conditions, however, there are significant discrepancies between the two sites, even when the wind is strong.

It is expected that the spatial relationship between the SST front and the wind direction can affect the airmass transformation in the KE region and the turbulent heat flux field. Therefore, we define two conditions correlated with the typical East Asian wintertime weather patterns, that is, the northerly wind conditions associated with the extraordinarily strong low pressure developing near the Kamchatka Peninsula (Chen et al. 1992; Yoshida and Asuma 2004; Bond and Cronin 2008), and the monsoon wind conditions associated with the strong northwesterlies of Siberian cold outbreaks (Suda 1957; Hsu and Wallace 1985, among others). Other times are characterized by frequent transitions in the weather pattern associated with the passage of highs and lows (Fig. 5), which do not cause such strong weather patterns. In particular, for this study, we identify the northerly wind condition as being when the wind direction is within 30° from 180° (in the oceanographic convention) and the wind speed is over 8.0 m s^{-1} , and the monsoon wind condition as being when the wind direction is within 30° from 110° and the wind speed is over 8.0 m s^{-1} . For a positive identification, these criteria must be satisfied for 60% of the wind records every 2 h and must last for more than a day at both KEO and JKEO. Supplemental weather charts are also considered. The rest of the period is grouped into the normal condition.

To determine the factors responsible for causing the simultaneous heat flux differences at KEO and JKEO, we evaluate terms (ii)–(iv) in Eqs. (1) and (2). The sequences of individual terms in Eqs. (1) and (2) are shown in Fig. 6. Term (iv) is very small throughout the period, which indicates that the spatial anomaly of the bulk coefficients caused by those of boundary layer parameters is systematically compensating each other.

It is true, however, that there are some periods when the spatial anomaly of the bulk coefficients [term (iv)] has some effect, such as on 4 and 9 March, during period I, and on 5 and 20 January, during period II, which are included in the normal condition. During these periods, term (iv) can become about 50% or more of term (ii) (Fig. 6), although the latent and the sensible heat fluxes at KEO and JKEO are about 200 W m^{-2} (except for the latent heat flux at JKEO on 5 January; see Fig. 3). Figure 6 also shows that the most prominent component producing the spatial anomaly of the heat flux is the wind speed anomaly expressed by term (iii). By closely looking at the wind speed difference between KEO and JKEO shown by Fig. 4, we find that the wind speed at KEO is as small as $1\text{--}2 \text{ m s}^{-1}$ during these periods. This condition helps to enlarge the term (iv), as U'_a is almost the same as U^{JKEO} and, therefore, term (iv) always reduces the effects of term (iii) for the total turbulent heat flux anomaly. Moreover, the unusually large value of term (iv) is due to the rapid increase of the bulk coefficients under the low wind speed below 3 m s^{-1} .

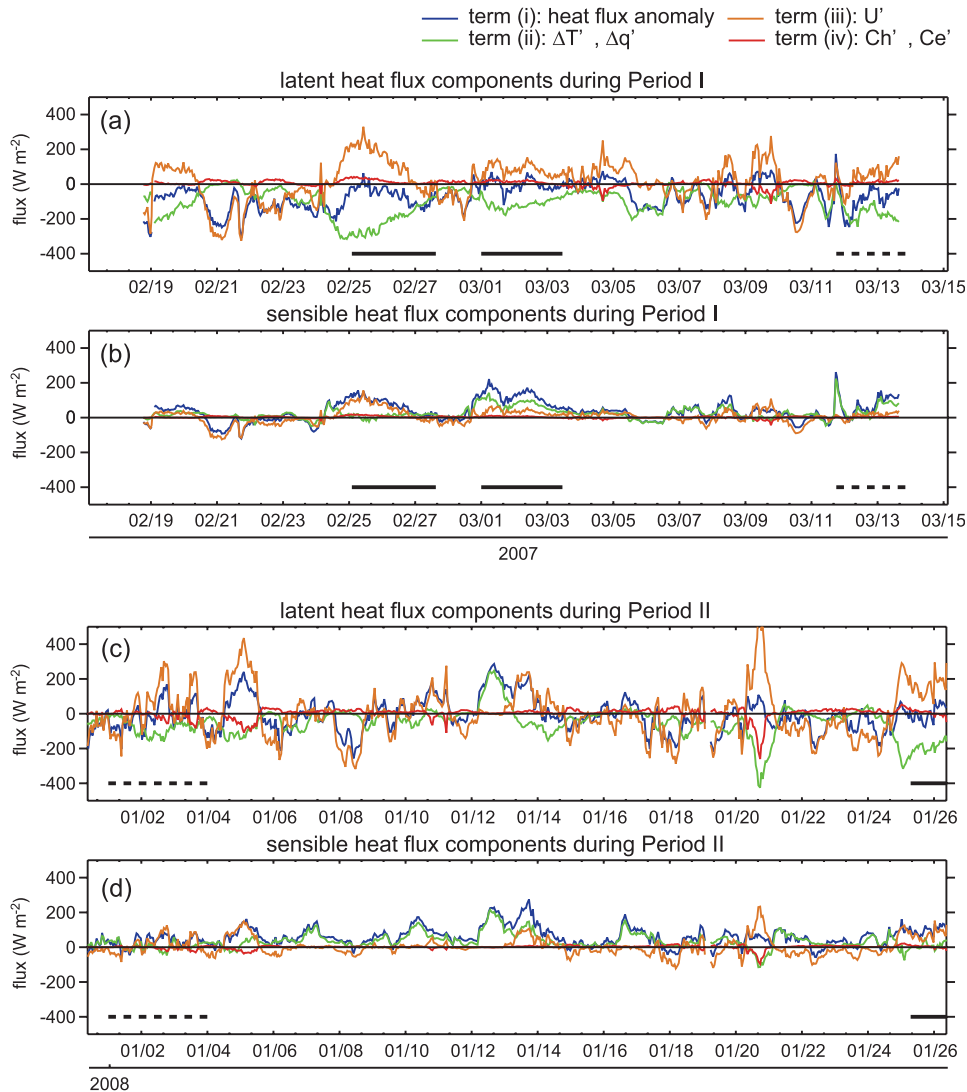


FIG. 6. Time series of the spatial anomaly components of the (a),(c) LHF and sensible (b),(d) SHF as indicated by Eqs. (1) and (2): (a),(b) 19 Feb to 15 Mar and (c),(d) 2 to 26 Jan. The blue line shows the spatial anomaly of the heat flux expressed by term (i), the green line shows the effects of the spatial anomaly of the ocean–atmosphere gradient in temperature (ΔT) and humidity (Δq) expressed by term (ii), and the orange line shows the effects of the wind anomaly expressed by term (iii). The red line shows term (iv), the spatial anomaly of the bulk coefficients. (a),(b) For period I; (c),(d) for period II, as in Fig. 3. Thick solid and broken lines indicate the period of the northerly wind condition and the monsoon wind condition, respectively.

Concerning the LHF during the northerly wind condition, the effects of the spatial anomaly of the air–sea gradient of the specific humidity [Δq ; see term (ii) in Eq. (2)] was almost balanced with that of the wind speed [term (iii) in Eq. (2)] during the northerly wind condition during periods I and II. This indicates that the effects of the wind speed in the downstream (KEO) were weaker than in the upstream (JKEO), while Δq was enlarged on the warm side of the front due to the nonlinear change of the saturated water vapor pressure given by the

Clausius–Clapeyron relation. This is the result of the airmass transformation that occurs as the cold air crosses the SST isotherms and attempts to restore to the warmer SST (Kondo 1976; Nonaka et al. 2009). When the adjustment of the ABL was very rapid, the ΔT to the south of the KE front was reduced, and term (ii) may increase, as seen during the second northerly wind condition during period I.

On the other hand, there remains the spatial difference in the SHF in the northerly wind condition. The term

TABLE 3. Average of the LHF and the SHF during the northerly wind condition, the monsoon wind condition, and the normal condition. The values are computed individually at KEO and JKEO during periods I and II.

		Period I		Period II	
		KEO	JKEO	KEO	JKEO
Northerly wind condition	Latent heat flux (W m^{-2})	385.1	351.7	401.2	402.6
	Sensible heat flux (W m^{-2})	157.2	255.2	184.2	285.3
Monsoon wind condition	Latent heat flux (W m^{-2})	382.3	300.3	303.6	285.6
	Sensible heat flux (W m^{-2})	102.1	183.7	106.1	138.4
Normal condition	Latent heat flux (W m^{-2})	240.8	155.1	233.4	218.4
	Sensible heat flux (W m^{-2})	68.4	81.0	68.6	124.9

balance in the first northerly wind condition during period I, as well as that during period II, show that the wind speed difference can influence the spatial anomaly of the SHF, as the value of term (ii) is reduced. In these cases, the air–sea temperature gradient ΔT on the north side of the SST front is almost the same as that on the south side, whereas the humidity gradient, Δq is larger. The second northerly wind condition during period I is characterized by the large contribution of term (ii). In this event, the SHF anomaly changes according to term (ii), whereas the wind speed at JKEO is larger than that at KEO (Fig. 4), as it is in the other events. The air–sea temperature gradient in the downstream area seems to be rapidly reduced due to the warming of the lower atmosphere by the warm sea surface. This is consistent with the previously mentioned airmass transformation across the SST front. Therefore, the relative importance of terms (ii) and (iii) in Eq.(1) might change, but the airmass transformation along the strong northerly wind stream is the key to this process, which can make up for the difference in the mechanism between the spatial anomaly of the SHF and that of the LHF.

Consequently, the LHF on each side of the KE front was simultaneously enhanced (Fig. 3), whereas the SHF on the northern side (JKEO) was larger under this weather condition. Recent numerical model studies have demonstrated an increase in the air temperature along the strong SST front associated with the growth of the ABL and the water vapor content along the cross-frontal wind (Spall 2007; Skillingstad and Edson 2009).

The temporal averages of the SHF and the LHF during the northerly wind conditions, monsoon conditions, and under normal conditions for both the 2007 and 2008 winter periods are tabulated in Table 3. During strong northerly wind conditions, LHF was remarkably large, with typical values of up to 400 W m^{-2} . Likewise, the SHF in the north was larger than that in the south by 100 W m^{-2} . These features were present during both periods I and II, although the absolute values of the fluxes differed slightly. A large heat input into the ABL helps to maintain the atmospheric baroclinicity, which dominates the storm-track activity in the northwest

Pacific (Nakamura et al. 2002). Nonaka et al. (2009) discuss the importance of the rapid equilibration of the cold atmosphere to the warm ocean surface across the SST front. However, the observational results here suggest that the equilibration to the warm ocean begins in the mixed water region north of the KE SST front, before the atmospheric mass crosses the KE SST front, and that the SHF gradually intensifies the atmospheric baroclinicity. This suggests that the SST front and the atmospheric weather conditions together contribute to the extremely large air–sea heat transfer in the KE region.

During the monsoon wind condition, there is a distinct difference in LHF and SHF between KEO and JKEO. The LHF to the south of the KE front is larger than that to the north, especially during period I, whereas the SHF to the south is much smaller than that to the north. As one can see from the wind directions at KEO and JKEO, the strong monsoon winds, which blow almost parallel to the strong SST front of the KE, undergo different airmass transformation processes over the cold and warm oceans. Siberian outbreaks are prominent during several days starting on 12 March during period I, and over 1–4 January during period II. It is noteworthy that term (ii) in Eqs. (1) and (2) seem to change independently (Fig. 6), whereas the wind speed and direction change almost simultaneously (Fig. 5).

As the air temperature is increased by the warm ocean surface south of the KE front, evaporation is enhanced due to the large Δq under the strong wind to the south of the KEO. In contrast, SHF north of the KE front is larger than the south. The sea surface cooling contrast across the KE front does not change very much, as the north–south differences of the SHF and the LHF tend to cancel each other out as indicated in Table 3.

For the rest of the period (the normal condition), the heat flux can be characterized by the generally larger evaporative cooling to the south of the KE front and weaker SHF to the south, on average, during period I. The contrast is relatively weak during period II. The relationship between the turbulent heat fluxes at KEO and JKEO is not systematic, as it frequently changes (almost on a daily time scale). There was a notable clockwise

rotation of the wind direction from 5 to 7 March during period I that is associated with the eastward passage of a low. When the southerly wind brought the warm atmosphere over the cold ocean, the evaporative cooling and the SHF were depressed despite the wind being strong (over 15 m s^{-1}) (Fig. 3a). This might be explained by the analogy of the warm atmosphere intrusion during the baiu season, as pointed out by Tanimoto et al. (2009). Figure 6a shows the rapid decrease of term (ii), which indicates the decrease of the moisture stratification, in Eq. (2). The spatial anomaly of the air–sea temperature difference indicated by term (ii) in Eq. (1) is slightly negative, as shown in Fig. 6b. These negative values indicate that the intrusion of the warm atmosphere over the cold ocean leads the weak stratification in the ABL to the north of the KE front and confines the large heat flux over the KE front in this condition.

It is evident from Fig. 3 that the SHF makes a large contribution to the ocean surface cooling and in turn to the thermal forcing of the ABL. The Bowen ratio (defined by H/Q) clearly shows that the energy balance in the ABL is quite different from that in the tropical ocean. The average of the Bowen ratio during period I (period II) was 0.55 (0.58) at JKEO, which is much larger than the typical value in the tropical ocean (0.1–0.3) (Pond et al. 1971). The averaged Bowen ratio at KEO during period I (period II) was 0.30 (0.29), which is as small as the ceiling cap of the typical tropical condition. That is because of the environment is in a cold regime to the north of the KE front and warm regime to the south, as shown in Fig. 4

The buoyancy forcing to the ABL increases to the south of the KE front because of a strong contrast in the Bowen ratio between the two sites, as pointed out by recent studies of the positive correlation between the ABL growth and the SST (Spall 2007; Skillingstad and Edson 2009), which implies the increase in the air temperature by the SHF between two buoys. This process can strengthen the frontal structure of the ABL on the KE front. It is true that the condition of turbulent heat flux on the KE front is not analyzed by these buoys. The spatially gridded data (such as the JCDAS dataset) are useful in spite of their low resolution in time and space.

c. Composite analysis

The analysis of the turbulent heat fluxes at KEO and JKEO in the previous subsection suggests that the spatial pattern of the turbulent heat flux in the KE region on monthly time scales is determined by the relative frequency of different types of wintertime weather conditions, each of which has a unique spatial relationship between the SST and the prevailing wind. To investigate this further, we conducted a composite analysis of the spatial pattern of the turbulent heat flux using the

reanalysis product of JCDAS. Composite maps of the turbulent heat flux during northerly wind conditions, monsoon wind conditions, and normal conditions during periods I and II are shown in Figs. 7a–c and 8a–c, as are the overall averages of the individual periods (Figs. 7d and 8d). The spatial characteristics of each condition are consistent with the interpretations of the spatial anomalies of the turbulent heat flux found between JKEO and KEO discussed in the previous subsection.

While the turbulent heat flux is remarkably large in the center of the KE region, the spatial distributions of the turbulent heat flux associated with different weather patterns are quite distinct. As indicated in Figs. 7a and 8a, during northerly wind conditions, the maximum value at the center of the KE is over 600 W m^{-2} along the frontal zone during period II and large values over 400 W m^{-2} extend meridionally on both sides of the KE. On the other hand, during monsoon wind conditions, when the cold outbreak blows off of Siberia, the maximum heat flux is confined to a narrow band along the Kuroshio and the western portion of the KE front (Figs. 7b and 8b). The turbulent heat flux in the KE region is generally smaller than during northerly wind conditions. Furthermore, during the monsoon conditions, the meridional change of the total turbulent heat flux across the KE front is as large. These features in individual weather patterns are common during periods I and II.

The spatial composite of the turbulent heat flux of the normal condition should be a reasonable one. The maximum heat flux is seen along the Kuroshio and KE because of the large ΔT and Δq values, which are the result of the cold atmosphere over the warm ocean during this season. On a monthly time scale, the average of the turbulent heat flux shown in Figs. 7d and 8d reflects to some extent this condition on average. However, it significantly differs in magnitude and in the place of the maximum value from the normal condition. It is evident that the area of the large heat flux over 300 W m^{-2} expands in the meridional direction, while the large heat flux is confined along the KE in Fig. 8d. It is also true that the area of 300 W m^{-2} ends near 160°E .

The relative frequency of occurrence of the northerly wind and the monsoon wind condition could be partially responsible for the significant discrepancy between the turbulent heat fluxes during periods I and II, as shown in Figs. 7d and 8d. Figure 3 clearly shows that the northerly wind condition occurs more during period I than in period II and that the northerly wind condition was rather short in period II. Furthermore, the monsoon wind condition was very strong in the beginning of period II, which may affect the monthly scale average. In this way, the relative occurrence of the different types of weather

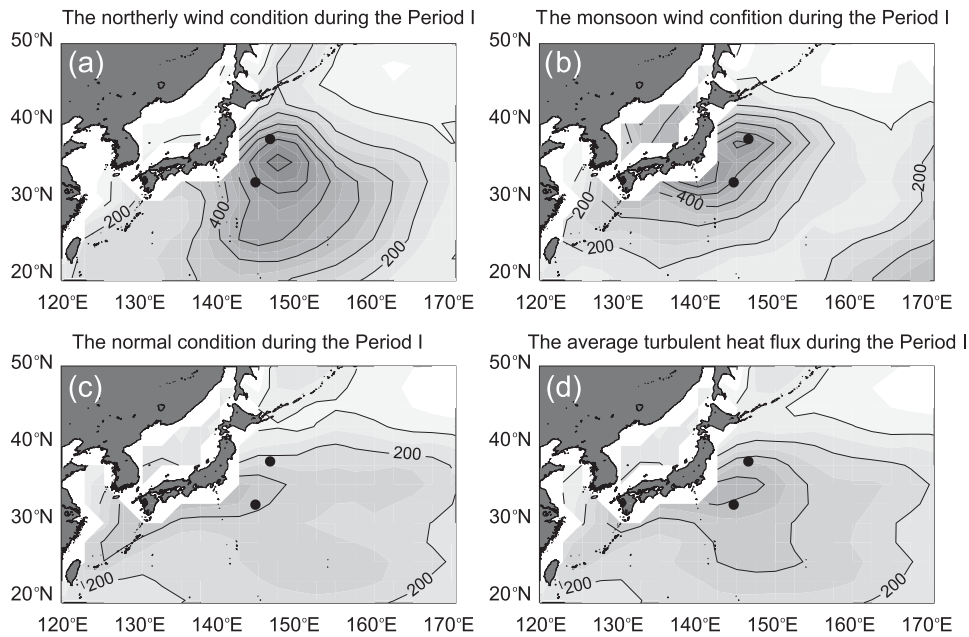


FIG. 7. Composites of the turbulent heat flux during (a) the northerly wind condition, (b) the monsoon wind condition, (c) the normal condition, and (d) the mean during period I, obtained from the JCDAS dataset. Units are W m^{-2} . The positions of KEO and JKEO are plotted by black circles.

conditions perhaps would strongly influence the spatial structure of the anomalously dominating heat flux for a given period.

d. Sensitivity analysis

Finally, we conducted a sensitivity analysis of the influence of the ABL parameters on the SHF and LHF.

The results suggest that the warm SSTs to the south of the KE strengthen the effects of the change of the wind speed. Each panel in Fig. 9 shows an example of the sensitivity of the LHF (SHF) to changes in the wind speed and the dewpoint temperature (air temperature) under a given condition of the SST (10° and 20°C) and a relative humidity of 70%. The average values of the

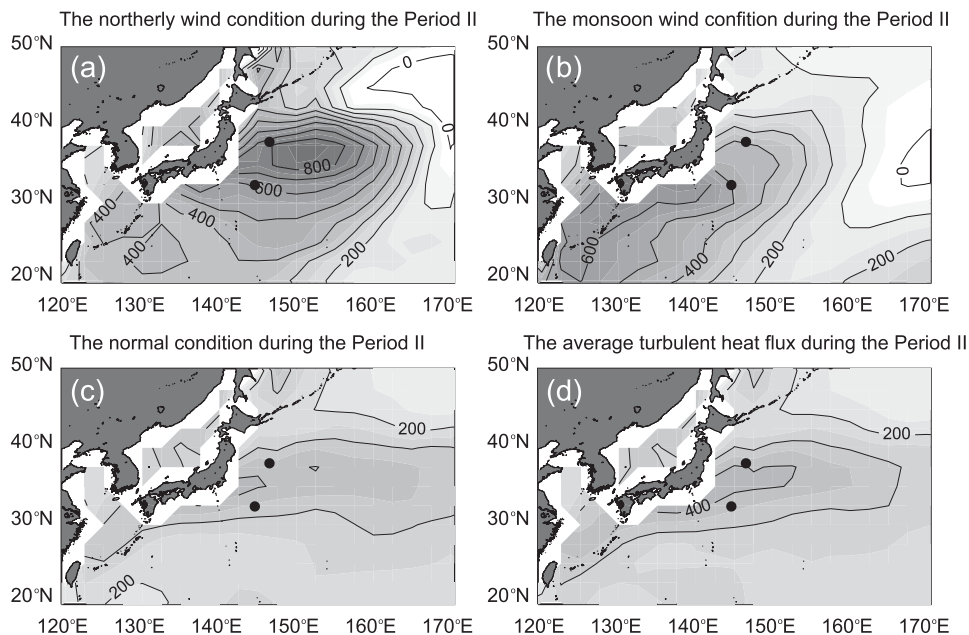


FIG. 8. As in Fig. 7, but for period II.

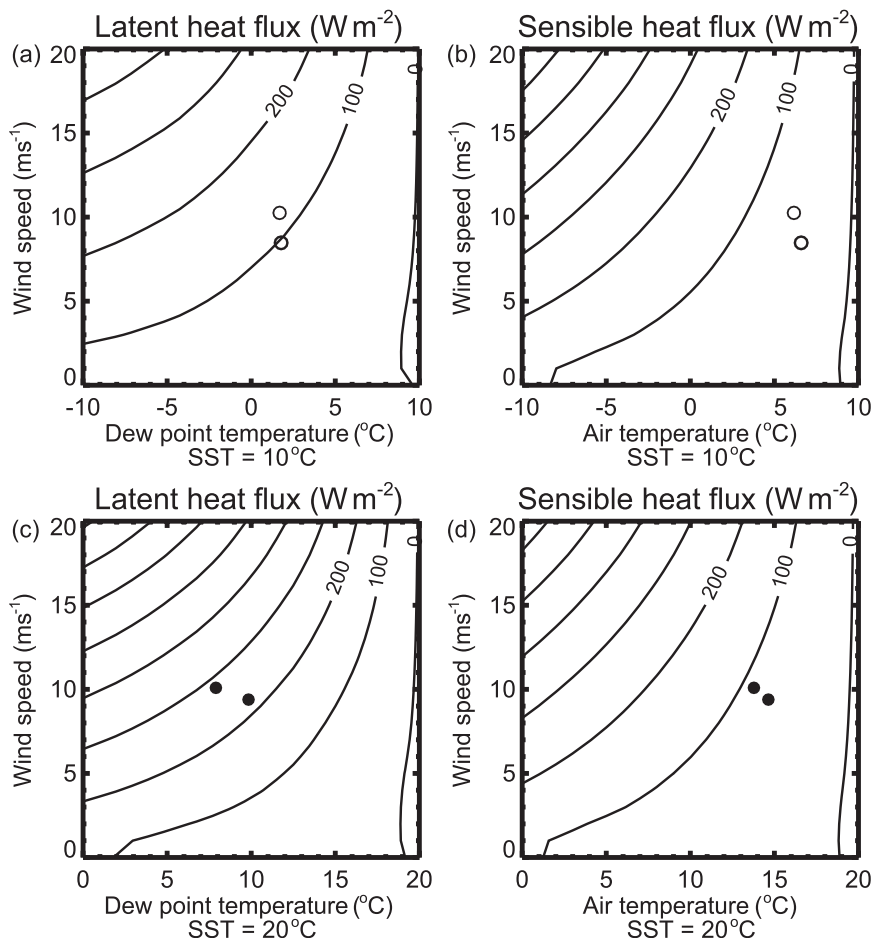


FIG. 9. The idealized sensitivity of the heat flux to the atmospheric conditions, using the COARE 3.0 bulk flux model (Fairall et al. 2003) under the conditions of (top) a cold SST of 10°C and (bottom) a warm SST of 20°C . The sensitivity of the LHF to the wind speed and the dewpoint temperature; (b),(d) as in (a),(c) but for the SHF to the wind speed and the air temperature. Conditions at KEO (filled circles) and JKEO (unfilled circles) are plotted approximately, considering the average values of the wind speed, dewpoint temperature, and the air temperature during periods I and II.

SST, dewpoint temperature, air temperature, and wind speed during periods I and II are, respectively, 12.7°C , 1.7°C , 6.2°C , and 10.3 m s^{-1} , and 14.0°C , 1.8°C , 6.6°C , and 8.5 m s^{-1} . Therefore, the conditions at JKEO are similar to the cold conditions shown in Figs. 9a and 9b. Those of KEO were 18.9°C , 7.9°C , 13.8°C , and 10.1 m s^{-1} , and 19.7°C , 9.8°C , 14.6°C , and 9.4 m s^{-1} , which are close to the conditions shown in Figs. 9c and 9d.

As shown in Figs. 9a and 9b, LHF is more sensitive to changes in the air–sea humidity gradient, Δq , during the warm conditions than during the cold conditions, as is expected when considering the nonlinear effects of the Clausius–Clapeyron relation. The reason for maintaining the large value of the LHF presumably can be attributed to the stronger sensitivity to the wind speed under the warm conditions.

In contrast, the sensitivity of the SHF does not change even though the SST range is different. This relation would support our contention that the strong wind and large ΔT contribute to the large heat release at the sea surface north of the KE front and that the nonlinear dependence of humidity on the air temperature helps to sustain the large heat flux with the warm sea surface and the rather weaker wind speed in the south of the KE region.

4. Discussion and concluding remarks

We have analyzed the winter surface heat flux variability and its difference between the north (JKEO) and the south (KEO) sides of the KE front on daily to synoptic time scales. The KEO buoy station has been located

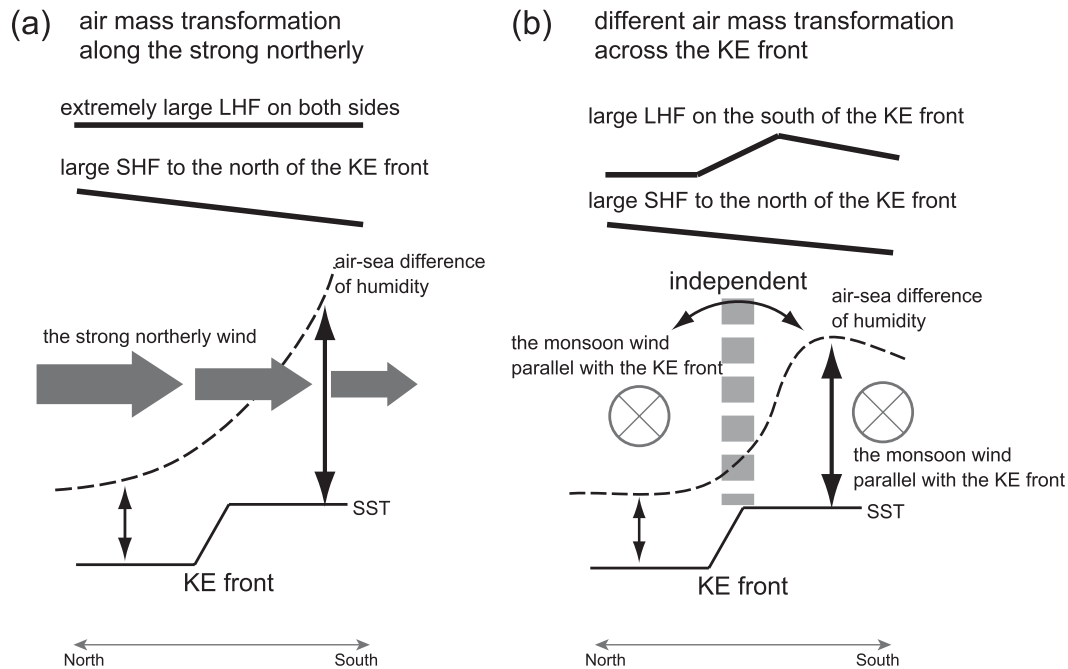


FIG. 10. Schematic views of the different airmass transformations across the KE front during (a) the northerly wind condition and (b) the monsoon wind condition. Also shown is the meridional cross section of the change in the ABL parameters and the LHF and SHF.

in the Kuroshio recirculation gyre south of the KE jet since June 2004. Measurements at the JKEO station, in the mixed water region north of the KE, began in February 2007. In this study we consider two winter periods of coincident observations at KEO and JKEO: period I, 18 February–12 March 2007, and period II, 1–25 January 2008.

During the wintertime, the SHF and the LHF were quite large both at KEO and at JKEO. It was found that the LHF eventually exceeds 400 W m^{-2} , while the SHF is also as large as $200\text{--}300 \text{ W m}^{-2}$. We found that these extreme conditions are produced in close relation with the speed and direction of the prevailing wind. We defined three weather conditions according to the wind strength and its direction: the northerly wind condition, the monsoon wind condition, and the normal condition.

As summarized in Fig. 10, the strong “northerly wind” pattern associated with a strong low pressure near the Kamchatka Peninsula is characterized by cross-frontal northerly wind and extraordinarily large turbulent heat fluxes, both to the north and south of the KE front. As a result of the airmass transformation along the prevailing wind, the large air–sea gradient in humidity (Δq) over the warm ocean south of the KE front can enhance the evaporative cooling, whereas the wind is stronger to the north (Fig. 10a). As a consequence, LHF shows little contrast across the KE front.

On the other hand, the SHF is larger to the north of the KE front than to the south. The air–sea transformation across the strong SST front leads the air–sea temperature gradient, ΔT , to decrease toward the downwind direction. The resultant spatial difference in the SHF should be both influenced by the wind speed anomaly and ΔT , although the relative importance of each can change.

The monsoon wind condition is also characterized by strong northwesterly wind and large heat fluxes in the KE region during both periods I and II. However, the spatial difference between the LHF and SHF did not seem to be systematic. The LHF to the north of the KE front was significantly smaller than that to the south at the end of period I because of the nonlinearly increasing air–sea gradient of humidity, while the spatial difference was not so large at the beginning of period II. As the prevailing wind is almost parallel with the KE front, changes in the heat fluxes on the north and south sides of the KE front are not necessarily simultaneous. That is, assuming it is natural for the SHF to the north of the KE front to be larger than that to the south (Fig. 10b).

During the normal condition, the maximum turbulent heat flux tends to be confined along the KE jet, and is generally smaller than the turbulent fluxes found during the other two weather patterns. This condition possibly

TABLE 4. Mean and standard deviation of the radiation fluxes during period I.

	Net LW radiation flux	SW radiation flux	Total radiation flux
KEO (W m^{-2})	15.2 ± 19.2	-229.7 ± 66.6	-214.5 ± 56.7
JKEO (W m^{-2})	71.9 ± 29.1	-108.3 ± 66.0	-36.4 ± 42.7

reflects the typical environment in the KE region, with the cold atmosphere over the warm current.

On the basis of a composite analysis of the 55-yr NCEP reanalysis product, Bond and Cronin (2008) suggested that interannual variations in the heat flux are dominated by SST rather than the atmospheric conditions. Our results suggest that the interannual changes in the relative occurrences of the different types of weather patterns can also cause interannual variations in the spatial distribution of the heat flux. The joint effects of the SST and the weather patterns should be further investigated to describe the year-to-year variations of the heat flux shown in Table 2.

The different spatial structures of the heat flux associated with different weather conditions proposed in this study highlight the basic fact that air–sea fluxes and atmospheric modification strongly depend on lateral advection that occurs during weather events. One of the important findings in this study is that the turbulent heat flux on nearly monthly time scales and its spatial distribution are closely related to the relative frequency of synoptic events. This result accentuates the importance of the high-frequency monitoring of the thermal air–sea interaction in the KE region.

The SST at JKEO can change by up to several degrees within a week, whereas the SST at KEO is relatively constant during winter. These different sensitivities might be related to changes in the oceanic mixed layer in mode water formation regions in the North Pacific (Oka et al. 2007). At KEO, the mixed layer in winter can extend down to about 400 m (Cronin et al. 2008), while the mixed layer depth is approximately 100 m at JKEO. In this analysis, the net surface heat flux is, for the most part, negative at the southerly buoy because of the solar insolation, whereas the net radiation flux is very small at the latitude of JKEO (Table 4). Such spatial variability suggests that the air–sea feedback process may have spatial dependence. However, careful analysis considering the lateral advection or the subduction processes is needed to demonstrate the oceanic feedback to the thermal forcing at the sea surface exactly.

An advantage of surface buoy measurements is that they highly resolve temporal variations. Their disadvantage is that they generally undersample the

spatial structure. For this, numerical model products and satellite measurements are better suited (Qiu et al. 2004; Kubota et al. 2008). As demonstrated in this analysis, however, the spatial structure depends upon capturing the synoptic temporal variability accurately, making the KEO and JKEO reference stations particularly valuable for validating these products (Konda et al. 2009).

Acknowledgments. The surface meteorological and oceanic data at KEO used in this study were provided by NOAA/PMEL. The data of JKEO were obtained from JAMSTEC/Research Institute for Global Change (RIGC). The observations from the JKEO buoy were achieved under the collaboration in research between JAMSTEC/RIGC and NOAA/PMEL. The reanalysis dataset used for this study was obtained through the cooperative research project of the JRA-25 long-term reanalysis by the Japan Meteorological Agency (JMA) and the Central Research Institute of Electric Power Industry (CRIEPI). The authors appreciate fruitful discussions with Akira Nagano, Hiroki Tokinaga, and Yasushi Karino. Comments and suggestions from three anonymous reviewers helped to clarify the focus of this manuscript. We also appreciate the cooperation of the crew of the R/V *Melville* for the deployment and the recovery of the KEO buoy and the R/V *Mirai* for the deployment and the recovery of the JKEO1 buoy. This study is partly supported by the Joint Research Program between Kyoto University and the Japan Aerospace Exploration Agency (Evaluation of the sea surface flux through the improvement of the wind speed derived by GCOM-W1 AMSR2).

REFERENCES

- Alexander, M. A., I. Bladé, M. Newman, J. R. Lanzante, N.-C. Lau, and J. D. Scott, 2002: The atmospheric bridge: The influence of ENSO teleconnections on air–sea interaction over the global oceans. *J. Climate*, **15**, 2205–2231.
- , L. Matrosova, C. Penland, J. D. Scott, and P. Chang, 2008: Forecasting Pacific SSTs: Linear inverse model predictions of the PDO. *J. Climate*, **21**, 385–402.
- Bond, N. A., and M. F. Cronin, 2008: Regional weather patterns during anomalous air–sea fluxes at the Kuroshio Extension Observatory (KEO). *J. Climate*, **21**, 1680–1697.
- , J. E. Overland, M. Spillane, and P. Stabenro, 2003: Recent shifts in the state of the North Pacific. *Geophys. Res. Lett.*, **30**, 2183, doi:10.1029/2003GL018697.
- Chen, S., 2008: The Kuroshio Extension front from satellite sea surface temperature measurements. *J. Oceanogr.*, **64**, 891–897.
- Chen, S.-J., Y.-H. Kuo, P.-Z. Zhang, and Q.-F. Bai, 1992: Climatology of explosive cyclones off the East Asian coastal cyclogenesis. *Mon. Wea. Rev.*, **120**, 3029–3035.

- Cronin, M. F., C. Meinig, C. L. Sabine, H. Ichikawa, and H. Tomita, 2008: Surface mooring network in the Kuroshio Extension. *IEEE Systems J.*, **2**, 424–430.
- Deser, C., M. A. Alexander, and M. S. Timlin, 1999: Evidence for a wind-driven intensification of the Kuroshio Current extension from the 1970s to the 1980s. *J. Climate*, **12**, 1697–1706.
- Di Lorenzo, E., and Coauthors, 2008: North Pacific gyre oscillation links ocean climate and ecosystem change. *Geophys. Res. Lett.*, **35**, L08607, doi:10.1029/2007GL032838.
- Fairall, C. W., E. F. Bradley, J. E. Hare, A. A. Grachev, and J. B. Edson, 2003: Bulk parameterization of air–sea fluxes: Updates and verification for the COARE algorithm. *J. Climate*, **16**, 571–591.
- Frankignoul, C., and N. Sennéchal, 2007: Observed influence of North Pacific SST anomalies on the atmospheric circulation. *J. Climate*, **20**, 592–606.
- Hsu, H.-H., and J. M. Wallace, 1985: Vertical structure of winter-time teleconnection patterns. *J. Atmos. Sci.*, **42**, 1693–1710.
- Joyce, T. M., I. Yasuda, Y. Hiroe, K. Koketsu, K. Kawasaki, and F. Bahr, 2001: Mixing in the meandering Kuroshio Extension and the formation of North Pacific Intermediate Water. *J. Geophys. Res.*, **106**, 4397–4404.
- Kalnay, E., and Coauthors, 1996: The NCEP/NCAR 40-Year Reanalysis Project. *Bull. Amer. Meteor. Soc.*, **77**, 437–471.
- Kara, A. B., P. A. Rochford, and H. E. Hurlburt, 2000: Mixed layer depth variability and barrier layer formation over the North Pacific Ocean. *J. Geophys. Res.*, **105**, 16 783–16 801.
- Kawai, H., 1972: Hydrography of the Kuroshio Extension. *Kuroshio, Its Physical Aspects*, H. Stommel and K. Yoshida, Eds., University of Tokyo Press, 235–352.
- Konda, M., N. Imasato, and A. Shibata, 1996: Analysis of the global relationship of biennial variation of sea surface temperature and air–sea heat flux using satellite data. *J. Oceanogr.*, **52**, 717–746.
- , H. Ichikawa, and H. Tomita, 2009: Wind speed and latent heat flux retrieved by simultaneous observation of multiple geophysical parameters by AMSR-E. *J. Remote Sens. Soc. Japan*, **29**, 191–198.
- Kondo, J., 1976: Heat balance of the East China Sea during the Air Mass Transformation Experiment. *J. Meteor. Soc. Japan*, **54**, 382–398.
- Kubota, M., A. Kano, H. Muramatsu, and H. Tomita, 2003: Intercomparison of various surface latent heat flux fields. *J. Climate*, **16**, 670–678.
- , N. Iwabe, M. F. Cronin, and H. Tomita, 2008: Surface heat fluxes from the NCEP/NCAR and NCEP/DOE reanalysis at the Kuroshio Extension Observatory buoy site. *J. Geophys. Res.*, **113**, C02009, doi:10.1029/2007JC004338.
- Kwon, Y.-O., and C. Deser, 2007: North Pacific decadal variability in the Community Climate System Model version 2. *J. Climate*, **20**, 2416–2433.
- Lau, N.-C., and M. J. Nath, 1994: A modeling study of the relative roles of tropical and extratropical SST anomalies in the variability of the global atmosphere–ocean system. *J. Climate*, **7**, 1184–1207.
- , and —, 1996: The role of the “atmospheric bridge” in linking tropical Pacific ENSO events to extratropical SST anomalies. *J. Climate*, **9**, 2036–2057.
- Lenschow, D. H., and E. M. Agee, 1976: Preliminary results from the Air Mass Transformation Experiment (AMTEX). *Bull. Amer. Meteor. Soc.*, **57**, 1346–1355.
- Liu, W. T., and C. Gautier, 1990: Thermal forcing on the tropical Pacific from satellite data. *J. Geophys. Res.*, **95**, 13 209–13 217.
- Liu, Z., and L. Wu, 2004: Atmospheric response to North Pacific SST: The role of ocean–atmosphere coupling. *J. Climate*, **17**, 1859–1882.
- Mantua, N. J., S. R. Hare, Y. Zhang, J. M. Wallace, and R. C. Francis, 1997: A Pacific interdecadal climate oscillation with impacts on salmon production. *Bull. Amer. Meteor. Soc.*, **78**, 1069–1079.
- Masuzawa, J., 1969: Subtropical mode water. *Deep-Sea Res.*, **16**, 463–472.
- McPhaden, M. J., 1995: The Tropical Atmosphere Ocean (TAO) array is completed. *Bull. Amer. Meteor. Soc.*, **76**, 739–741.
- Murakami, H., and H. Kawamura, 2001: Relations between sea surface temperature and air–sea heat flux at periods from 1 day to 1 year observed at ocean buoy stations around Japan. *J. Oceanogr.*, **57**, 565–580.
- Nakamura, H., T. Izumi, and T. Sampe, 2002: Interannual and decadal modulations recently observed in the Pacific storm track activity and East Asian winter monsoon. *J. Climate*, **15**, 1855–1874.
- , T. Sampe, A. Goto, W. Ohfuchi, and S.-P. Xie, 2008: On the importance of mid-latitude oceanic frontal zones for the mean state and dominant variability in the tropospheric circulation. *Geophys. Res. Lett.*, **35**, L10079, doi:10.1029/2008GL034010.
- Ninomiya, K., and H. Mizuno, 1985: Anomalous cold spell in summer over northeastern Japan caused by northeasterly wind from polar maritime air mass. Part I. EOF analysis of temperature variation in relation to the large-scale situation causing the cold summer. *J. Meteor. Soc. Japan*, **63**, 845–857.
- Nonaka, M., and S. P. Xie, 2003: Covariations of sea surface temperature and wind over the Kuroshio and its extension: Evidence for ocean-to-atmosphere feedback. *J. Climate*, **16**, 1404–1413.
- , H. Nakamura, B. Taguchi, N. Komori, A. Kuwano-Yoshida, and K. Takaya, 2009: Air–sea heat exchanges characteristic to a prominent midlatitude oceanic front in the South Indian Ocean as simulated in a high-resolution coupled GCM. *J. Climate*, **22**, 6515–6535.
- Oka, E., L. D. Talley, and T. Suga, 2007: Temporal variability of winter mixed layer in the mid- to high-latitude North Pacific. *J. Oceanogr.*, **63**, 293–307.
- Onogi, K., and Coauthors, 2007: The JRA-25 reanalysis. *J. Meteor. Soc. Japan*, **85**, 369–432.
- Pond, S., G. T. Phelps, J. E. Paquin, G. McBean, and R. W. Stewart, 1971: Measurements of the turbulent fluxes of momentum, moisture and sensible heat over the ocean. *J. Atmos. Sci.*, **28**, 901–917.
- Qiu, B., S. Chen, and P. Hacker, 2004: Synoptic-scale air–sea flux forcing in the western North Pacific: Observations and their impact on SST and the mixed layer. *J. Phys. Oceanogr.*, **34**, 2148–2159.
- Skyllingstad, E. D., and J. B. Edson, 2009: Large-eddy simulation of moist convection during a cold air outbreak over the Gulf Stream. *J. Atmos. Sci.*, **66**, 1274–1293.
- Spall, M. A., 2007: Midlatitude wind stress–sea surface temperature coupling in the vicinity of oceanic fronts. *J. Climate*, **20**, 3785–3801.
- Suda, K., 1957: The mean pressure field characteristic to persistent cold waves in the Far East. *J. Meteor. Soc. Japan*, **35** (75th Anniversary Vol.), 192–198.
- Suga, T., and K. Hanawa, 1990: The mixed layer climatology in the northwestern part of the North Pacific subtropical gyre and the formation area of Subtropical Mode Water. *J. Mar. Res.*, **48**, 543–566.

- , and —, 1995: Interannual variations of North Pacific Subtropical Mode Water in the 137°E section. *J. Phys. Oceanogr.*, **25**, 958–970.
- Talley, L., 1993: Distribution and formation of North Pacific intermediate water. *J. Phys. Oceanogr.*, **23**, 517–537.
- Tanimoto, Y., N. Iwasaka, K. Hanawa, and Y. Toba, 1993: Characteristic variations of sea surface temperature with multiple time scales in the North Pacific. *J. Climate*, **6**, 1153–1160.
- , S.-P. Xie, K. Kai, H. Okajima, H. Tokinaga, T. Murayama, M. Nonaka, and H. Nakamura, 2009: Observations of marine atmospheric boundary layer transitions across the summer Kuroshio Extension. *J. Climate*, **22**, 1360–1374.
- Tokinaga, H., and Coauthors, 2006: Atmospheric sounding over the winter Kuroshio Extension: Effect of surface stability on atmospheric boundary layer structure. *Geophys. Res. Lett.*, **33**, L04703, doi:10.1029/2005GL025102.
- Yasuda, I., 1997: The origin of the North Pacific Intermediate Water. *J. Geophys. Res.*, **102**, 893–909.
- Yoshida, A., and Y. Asuma, 2004: Structures and environment of explosively developing extratropical cyclones in the northwestern Pacific region. *Mon. Wea. Rev.*, **132**, 1121–1142.